Hindawi
International Journal of Antennas and Propagation
Volume 2018, Article ID 7068560, 7 pages
https://doi.org/10.1155/2018/7068560

Research Article

Axial Ratio-Tuned Circularly Polarized Square Patch Antenna with Long Stubs

Y. Sung

Kyonggi University, Republic of Korea

Correspondence should be addressed to Y. Sung; yjsung@kgu.ac.kr

Received 19 July 2018; Revised 4 September 2018; Accepted 12 September 2018; Published 25 November 2018

Academic Editor: N. Nasimuddin

In this letter, we propose a circularly polarized (CP) square antenna that can change the frequency of the minimum axial ratio (AR). The proposed antenna is designed in a very straightforward manner by applying four long stubs to a square patch. The length of one of the stubs is different from that of the other three stubs, and the structural asymmetry is realized in such a manner that the CP characteristic is conveniently obtained. The proposed antenna can independently adjust the resonant frequency and the frequency of the minimum AR value. Therefore, the resonant frequency and the frequency at which the minimum AR value appears can be easily matched. By applying this method, six antennas with the adequate CP characteristic, notwithstanding the varied stub widths (1.5~6.5 mm), are designed.

1. Introduction

With the rapid development of wireless mobile communication, a large amount of information regardless of time and place is exchanged [1], making the maintenance of the signal connection between the transmitter and receiver during communication indispensable [2]. There are numerous reasons for call drop during communication, one of them being the change in polarization. In urban areas, the number of buildings present is large. The polarization axis of the propagation wave can be changed as it impinges on these objects and is transmitted or reflected [3, 4]. Therefore, it is challenging for appropriate polarization to reach the receiver [5].

Circularly polarized (CP) antennas are relatively insensitive to the direction of polarization when compared with linear polarized (LP) antennas; thus, they can be received irrespective of the polarization direction [6]. Therefore, CP antennas are robust against multipath interference and are less affected by Faraday rotation [7].

A common method to obtain the CP characteristic using a square patch is to cut out [8, 9] a portion of the corner located at ±45° relative to the feed point or vice versa to add a very short stub [10]. Owing to this asymmetry, LP is formed along the two diagonal lines. The resonant frequencies of the two LP waves are adjacent, and their magnitudes are very similar. In this case, the phase difference is 90° as the two polarized waves are perpendicular to each other; thus, the CP characteristic can be obtained. The antenna proposed in this letter is structurally different from the previous works [8–12] in two respects. First, the stub length is used to obtain the CP property, and it is relatively long compared to conventional structures. Second, CP can be obtained notwithstanding whether the stub is not located on the diagonal line with respect to the feeding point.

As is well known, the operating bandwidth of a CP antenna is defined as a frequency band in which the bandwidth where $|S_{11}| \leq -10$ dB and that where axial ratio (AR) ≤ 3 dB overlap. Conventional CP antennas exhibit a shortcoming in that the bandwidth is reduced when the resonant frequency in the S_{11} graph and the minimum point of the AR graph are different. The most prominent feature of the proposed structure is that it can independently adjust the resonant frequency and the frequency of the minimum point AR. Based on this method, an antenna with the CP characteristic is efficiently designed.

In order to compare the proposed antenna in this work with previously reported single-feed circularly polarized antennas, the size, gain, and measured BWs of the antennas

are summarized in Table 1. Compared with the previously presented circularly polarized antennas, the 3 dB AR BW of the proposed antenna is similar or enhanced. The antennas with a larger AR BW than the proposed antenna are [13, 14]. However, these antennas exhibited a high profile greater than 15 mm. In [15], a cross slot in the ground plane was used to decrease the resonant frequency and obtain size reduction. However, there is a problem that the back radiation is generated due to the slot of the ground plane and the gain is low. An asymmetric-circular shaped slotted square microstrip patch antenna for the CP radiation was proposed in [16]. However, the gain is very low, 0.5 dBic, and the profile is somewhat thick with 4.8 mm. To achieve CP radiation and antenna size reductions, an arrowhead-shaped slot is embedded in a square patch [17]. However, AR bandwidth of the antenna is too narrow. In [18], a wide coverage CP antenna over 180 degrees was proposed, but its size is twice as large as the proposed antennas. Until recently, there has been little research on the technique of tuning AR even in the field of CP antennas. In the dual-feed CP antenna, the direction of the minimum AR was steered by adjusting the phase difference applied to the two feeds [19]. To the best of my knowledge, adjusting the frequency of the minimum AR is a novel technology that has not been reported previously.

The rest of this paper is organized as follows. Section 2 describes the antenna geometry. Operating principle and parameter study are in Sections 3 and 4, respectively. Simulation and measurement results for the proposed antenna are given in Section 5. The conclusions are provided in Section 6.

2. Antenna Geometry

Figure 1 shows the proposed CP antenna. The antenna proposed here is fabricated on a substrate of thickness $h = 1.57$ mm with relative permittivity $\varepsilon_r = 2.2$. Four L-shaped stubs are applied onto the square patch rotated by 45°. Its side length is A. A similar CP characteristic can be obtained by straight line stubs; however, bent stubs are selected to efficient space utilization. The four stub widths are set to w. Two stubs (stub 1 and stub 2) move by d from the top vertex of the square, and the remaining two stubs (stub 3 and stub 4) move equally with respect to the bottom vertex. The length of stub 4 located at the bottom-right is set to L_2, and the length of the remaining three stubs is set to L_1. The width and position of the four stubs remain the same, and the asymmetric structure is formed only by the stub length difference. Finally, CP performance is realized.

The proposed antenna is fed by a CPW line, as shown in Figure 1(b). It consists of a 50 Ω line (linewidth = 3 mm and gap = 0.5 mm) and matching section ($L_m \times W_m$). The gray region except for the nonground area ($L_f \times W_f$) functions as the ground plane. The width W_m is set to 0.7 mm, which corresponds to approximately 151 Ω. The length L_m is 32.3 mm, which corresponds to a length of approximately $\lambda_g/4$ at the operating frequency. The matching section straightforwardly acts as a quarter-wavelength transformer. The nonground region is at a distance s from the top edge.

Table 1: Comparison of conventional single-feed circularly polarized antennas.

Ant.	10 dB S_{11} BW	3 dB AR BW	Size	Height	Gain
This work	1.2%	2.3%	$0.20\lambda_0 \times 0.20\lambda_0$	1.6 mm	3.6 dBi
[13]	10.9%	2.8%	$0.25\lambda_0 \times 0.25\lambda_0$	20 mm	4.75 dBi
[15]	6.1%	1.6%	$0.18\lambda_0 \times 0.18\lambda_0$	1.52 mm	2.5 dBi
[16]	4.01%	1.2%	$0.27\lambda_0 \times 0.27\lambda_0$	4.8 mm	0.5 dBic
[17]	3.8%	0.8%	$0.26\lambda_0 \times 0.26\lambda_0$	4.5 mm	4.55 dBi
[14]	20.81%	2.6%	$0.24\lambda_0 \times 0.24\lambda_0$	15.6 mm	6.9 dBi
[18]	4.3%	2.1%	$0.48\lambda_0 \times 0.48\lambda_0$	1.6 mm	4.5 dBic

The distance between the feed and the ground plane is fixed to the value shown in Figure 1(b), and these values are optimal results obtained by performing iterative simulations. Simulation is carried out using HFSS. The size of the substrate is $70 \times 70\ \text{mm}^2$.

3. Operating Principle

In order to understand the operating principle of the proposed antenna, the antenna is rotated counterclockwise with respect to the center. The other parameters are as follows: $A = 15.6$ mm, $w = 4.5$ mm, $L_1 = 11.5$ mm, $L_2 = 10.7$ mm, $s = 11.6$ mm, $d = 0.6$ mm, $L_f = 36.5$ mm, $W_f = 4$ mm, $L_m = 32.3$ mm, and $W_m = 0.7$ mm. Here, α is the rotated angle of the antenna. The dotted line is the antenna shown in Figure 1, and the gray shading structure with a solid outline is a rotated antenna. As the rotation angle α increases, the two resonant frequencies split further. When the rotation angle α is less than 25°, two resonances are located close together and appear as a single resonance on the graph. When the rotation angle α is over 25°, the second resonance appears weak; however, the rotated antenna displays dual resonance. As is well known, CP is a combination of two LPs located perpendicular to each other. To verify this, we will examine the E-field distribution formed at two resonant frequencies.

Figure 2 shows the simulated E-field at 2.244 and 2.656 GHz, corresponding to two resonant frequencies of the proposed antenna with $\alpha = 40°$. The darker area is the stronger E-field, and the brighter area is the weaker E-field. In Figure 2(a), the electric field is strongly formed based on the null line formed along the right diagonal line. In Figure 2(b), the electric field is formed strongly based on the null line formed along the left diagonal line. Thus, it is observed that the electric field distributions at the two resonance frequencies are orthogonal to each other with respect to the null line. The appearance of the relatively weak E-field at the second resonance frequency is owing to the weakly formed resonance, as shown in Figure 3. Based on these facts, it can be inferred that the proposed structure combines two resonance modes perpendicular to each other to exhibit CP characteristics.

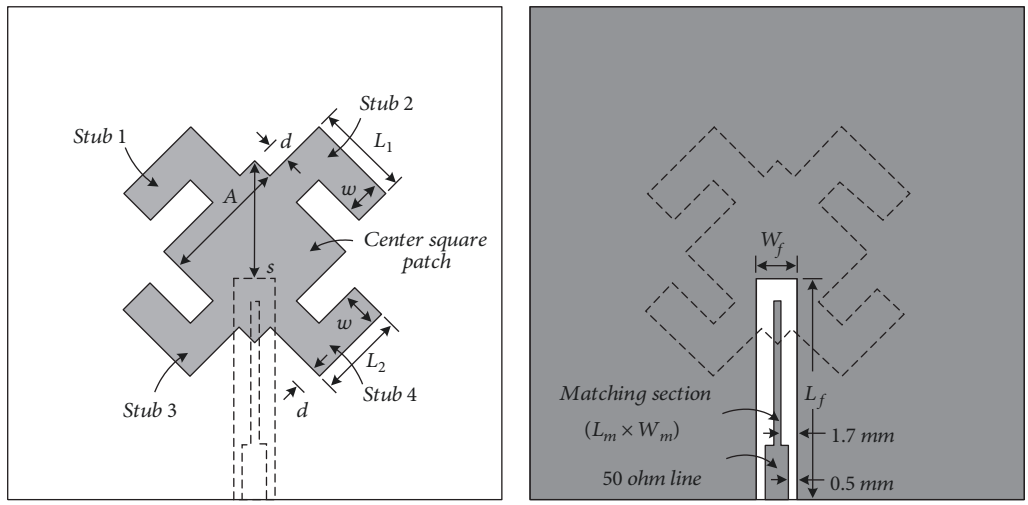

Figure 1: Proposed circularly polarized antenna: (a) top layer and (b) bottom layer viewed from above.

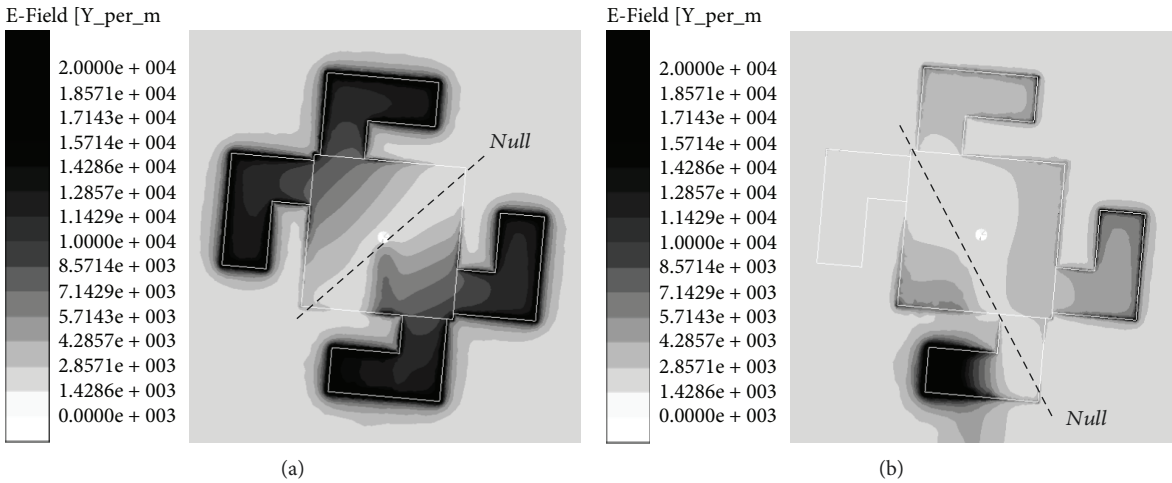

Figure 2: Simulated E-field distribution: (a) 2.244 GHz and (b) 2.656 GHz.

4. Parameter Study

Figure 4 shows the simulated results of the reflection coefficient, AR, and phase difference of the two resonant frequencies with respect to the stub position d. The remaining parameters are identical to those mentioned above. Here, d is the distance from the vertex of the stub, and all the four stubs are identical. As d increases, the resonant frequency increases, and the impedance matching characteristic tends to improve. Generally, in the patch antenna, an E-field exists strongly in the vicinity of the feed point and in that of the opposite side of the feed point. In the proposed antenna, an upper vertex and a lower vertex correspond to this area. As the stub shifts away from the upper or lower vertex, the E-field weakens such that the E-field applied to the stub also weakens. If the stub is located at the right and left vertices, the resonant frequency is changed negligibly. That is, the stub length does not contribute substantially to reducing the resonant frequency. However, as the stub shifts closer to the upper and lower vertices, where a strong electric field appears, the E-field applied to the stub is strong such that the resonant frequency is strongly influenced by the stub length. In addition, the stub is embedded into the strong E-field region such that the impedance matching is deteriorated.

As d increases, the frequency of the minimum AR remains unchanged within a small margin of error, and only the minimum value of the AR becomes worse. As shown in Figure 4(c), the frequency response of the phase difference changes negligibly with d. Therefore, the frequency at which the phase difference becomes 90° is nearly unchanged. Consequently, the minimum AR frequency is nearly unchanged as well. Because the resonant frequency formed on the basis of the reflection coefficient and the frequency at which the minimum point of AR should coincide, d is selected to be 0.6 mm. From the simulated results, it is observed that d can be used as a parameter to change only the resonant frequency of the antenna.

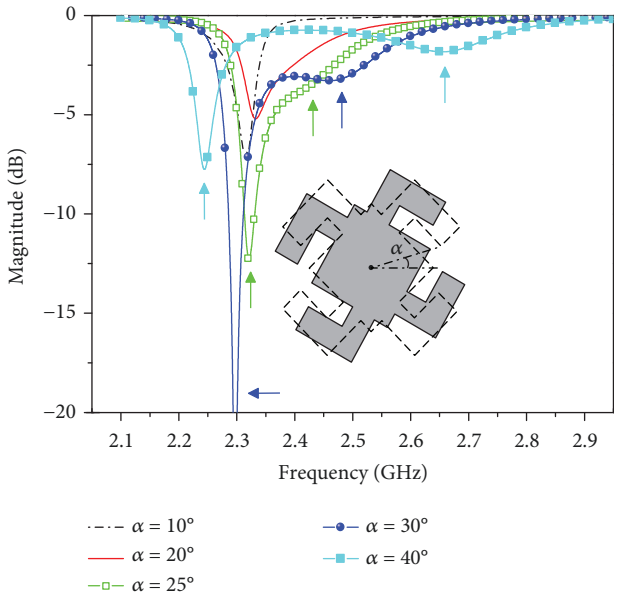

Figure 3: Simulated reflection coefficient of the proposed antenna with different rotated angles α.

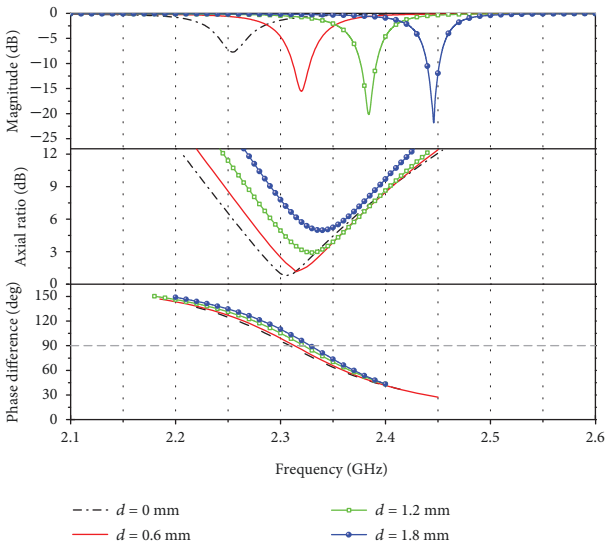

Figure 4: Simulated results of the proposed antenna with different positions d: reflection coefficient, AR, and phase difference between two resonant frequencies.

Figure 5 shows the simulated results of the reflection coefficient and AR characteristics according to the change of s. All the other parameters are set equal to those mentioned above. In this study, s affects only impedance matching and exerts negligible effect on the resonant frequency, as shown in Figure 5(a). However, the frequency response of AR shifts downward as s increases, as shown in Figure 5(b). At this time, the optimum s is 11.53 mm. Figure 5(c) shows the simulated result of the phase difference of the two resonance modes according to the change of s. It is observed that as s increases, the frequency at which the phase difference becomes 90° decreases. In addition, the frequency at which

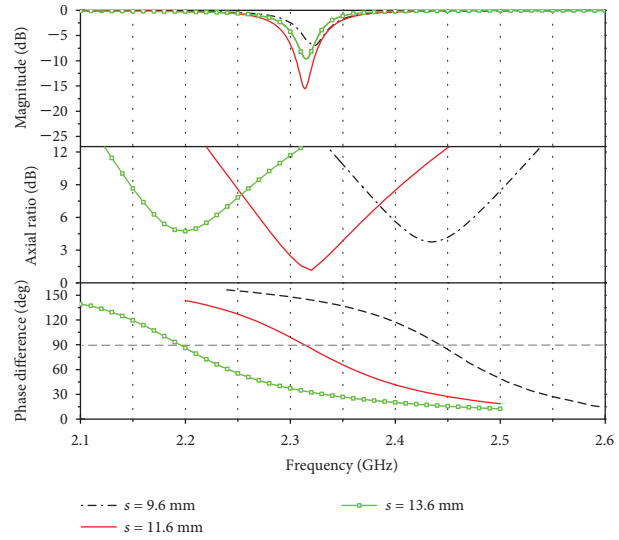

Figure 5: Simulated results of the proposed antenna with different distances s: reflection coefficient, AR, and phase difference of two resonant frequencies.

the phase difference becomes 90° almost coincides with the frequency having the minimum point on the AR graph. s is a variable that can independently move the position of the minimum AR point.

Figure 6 shows the simulated results of reflection coefficient and AR characteristics according to the change of L_1. All the other variables are set equal to those mentioned above. At this time, in order to maintain proper asymmetry, the length variation of L_2 is identical to that of L_1. As the stub length varies, the resonant frequency and the minimum point of the AR always coincide. Impedance matching deteriorates with increasing length L_1, and AR is optimum when $L_1 = 12.5$ mm. Considering the S_{11} characteristic, L_1 is selected to be 11.5 mm.

Conventional CP antennas have a limited design range for perturbations such as corner-cuts or stubs. If the perturbation is small, the adjacent two resonances cannot be split. On the contrary, if the perturbation is large, the two resonances are split excessively, and the antenna exhibits a dual-band LP characteristic. On the other hand, as shown in Figure 6, the proposed structure exhibits a considerably wide design range of the stub for the CP characteristic.

The design procedure for implementing the CP characteristic using the proposed technique can be summarized as follows:

(1) Apply four identical L-shaped stubs to a square patch. At this time, i.e., when the procedure begins, d is set to 0 mm

(2) Reduce the length of the bottom-right stub and verify if the AR value reduces to below 3 dB

(3) Change d or s to coincide two resonant frequencies (frequency of the minimum AR value and resonant frequency of the antenna)

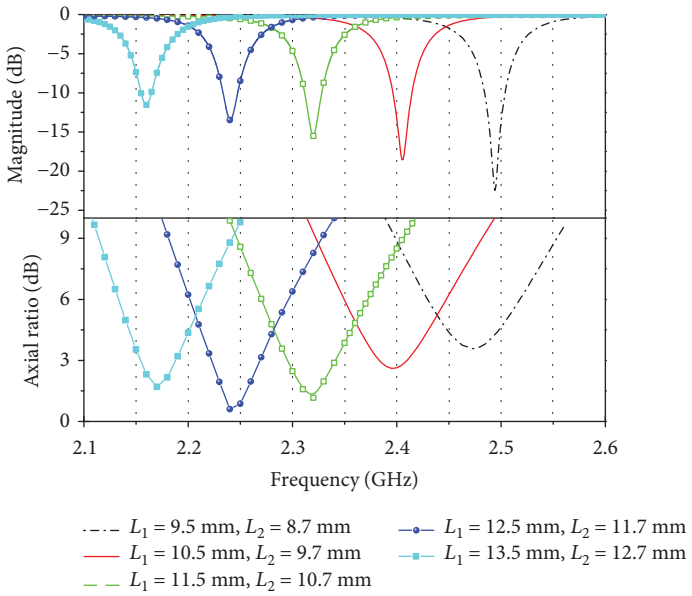

Figure 6: Simulated results of the proposed antenna with different lengths L_1: reflection coefficient and AR.

Table 2: Optimal design parameters and performance of the CP antenna with different stub widths.

w	A	d	s	L_1	L_2	$S_{11} < -10$ dB	AR < 3 dB
1.5	15.6	1.7	10.8	11.5	10.7	2.286~2.304	2.267~2.310
2.5	15.6	1.7	11.6	11.5	10.7	2.297~2.314	2.284~2.328
3.5	15.6	1.1	11.6	11.5	10.7	2.287~2.304	2.277~2.326
4.5	15.6	0.6	11.6	11.5	10.7	2.312~2.328	2.295~2.342
5.5	15.6	0	11.6	12.5	11.5	2.272~2.293	2.250~2.311
6.5	15.6	0	12.9	12.5	11.2	2.405~2.429	2.412~2.460

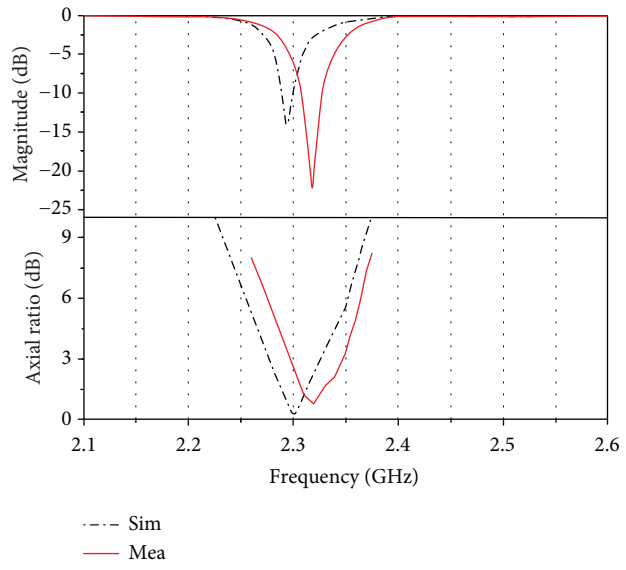

Figure 7: Simulated and measured results of the proposed antenna: reflection coefficient and AR.

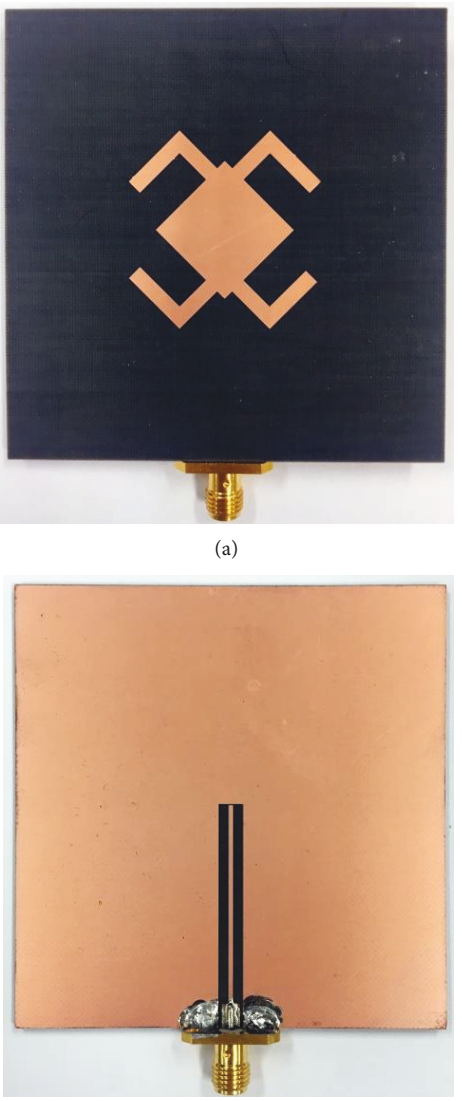

Figure 8: Picture of the fabricated antenna: (a) top layer and (b) bottom layer.

(4) Adjust L_1 (and L_2) to regulate the operating frequency of the CP antenna

(5) Tune the feeding part to optimize impedance matching

Six CP antennas with various stub widths are designed according to the above process. The design parameters presented in Table 1 are obtained based on the final antenna ($w = 4.5$ mm). That is, the minimum AR frequency and the resonant frequency are rendered different by reducing or increasing the stub width w of the antenna, with $w = 4.5$ mm; moreover, the two resonant frequencies can be reconciled again by minimizing changes in the other parameters. Therefore, the design parameters d, s, and L_1 for a certain w can be various combinations apart from the values presented in Table 2.

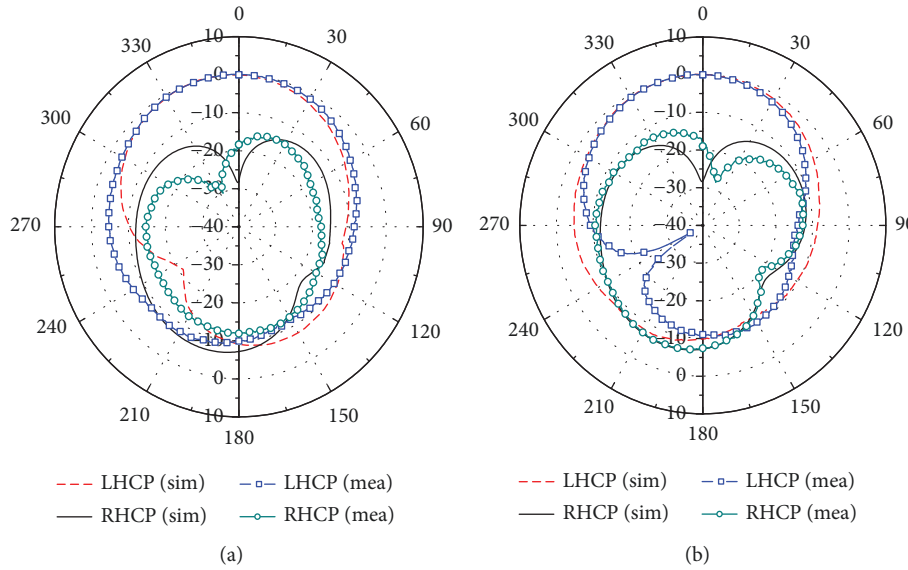

Figure 9: Simulated and measured radiation patterns: (a) xz plane and (b) yz plane.

5. Simulated and Measured Results

Figure 7 shows the measured and simulated frequency responses for the proposed antenna. The proposed antenna is fabricated on a Duroid 5880 substrate with $h = 1.57$ mm and $\varepsilon_r = 2.2$. The geometric dimensions of the proposed antenna are as follows: $A = 15.6$ mm, $w = 4.5$ mm, $\alpha = 40^\circ$, $L_1 = 11.5$ mm, $L_2 = 10.7$ mm, $d = 0.6$ mm, $s = 11.6$ mm, $L_f = 36.5$ mm, $W_f = 4$ mm, $L_m = 32.3$ mm, and $W_m = 0.7$ mm. Experiments verify that the characteristics of the proposed antenna are consistent with the simulation results. The deviation between the simulated and measured results may be caused by the loss tangent of the substrate and the parasitic effects of the SMA connectors. The measured impedance bandwidth (10 dB reflection coefficient) is 1.2%. The measured 3 dB axial ratio bandwidth of the proposed antenna is 2.3%. Figure 8 shows the photographs of the fabricated antenna.

We set the double ridged horn antenna as Tx antenna and the proposed antenna as Rx antenna. At this time, Tx antenna is an LP antenna. After measuring the vertical polarization (E_x) and the horizontal polarization (E_y), AR value is computed using the following equation [20]:

$$E_{\mathrm{RHCP}} = \frac{1}{\sqrt{2}}\left(E_x + jE_y\right),$$
$$E_{\mathrm{LHCP}} = \frac{1}{\sqrt{2}}\left(E_x - jE_y\right), \quad (1)$$
$$\mathrm{AR} = -\frac{\left(|E_{\mathrm{RHCP}}| + |E_{\mathrm{LHCP}}|\right)}{\left(|E_{\mathrm{RHCP}}| - |E_{\mathrm{LHCP}}|\right)}.$$

Figure 9 shows the plot of the simulated and measured radiation patterns. The maximum gain is 3.6 dBic. The measurement results demonstrate that a broadside radiation pattern with a good left-handed CP (LHCP) characteristic is obtained at the resonant frequency. Figure 10 shows the simulated and measured gains of the proposed antenna.

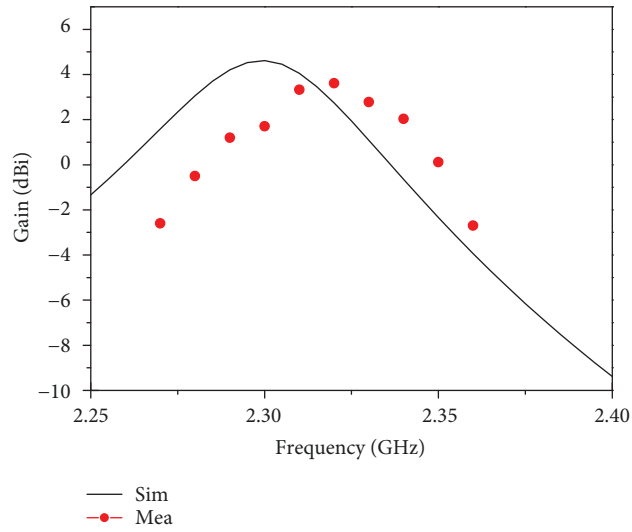

Figure 10: Simulated and measured gains.

6. Conclusion

A novel CP antenna is proposed to independently adjust the frequency of the minimum AR point. The proposed structure consists of a square patch and four stubs, and the CP characteristic is realized by the difference in the length of the stubs. In this study, the position of the stub is the resonant frequency of S_{11}, and the length of the nonground area in the feed structure is a variable that can tune the frequency of the minimum AR independently. As the stub width is varied, the positions of the two frequencies (the resonant frequency and the frequency of the minimum AR) are arbitrarily

changed. However, based on the proposed method, positions of the two frequencies are easily matched. The operating principle of the proposed antenna is exploited, and a design strategy is provided for the antenna.

Data Availability

The data used to support the findings of this study are included within the article.

Conflicts of Interest

The authors declare that they have no conflicts of interest.

Acknowledgments

This work was supported by the National Research Foundation Grant funded by the Korean Government under Grant 2017R1A2B4010393.

References

[1] S. Xiao, X. Zhou, D. Feng, Y. Yuan-Wu, G. Y. Li, and W. Guo, "Energy-efficient mobile association in heterogeneous networks with device-to-device communications," *IEEE Transactions on Wireless Communications*, vol. 15, no. 8, pp. 5260–5271, 2016.

[2] J. F. Valenzuela-Valdes, M. A. Garcia-Fernandez, A. M. Martinez-Gonzalez, and D. A. Sanchez-Hernandez, "Evaluation of true polarization diversity for MIMO systems," *IEEE Transactions on Antennas and Propagation*, vol. 57, no. 9, pp. 2746–2755, 2009.

[3] X. Li, X. Huang, Z. Nie, and Y. Zhang, "Equivalent relations between interchannel coupling and antenna polarization coupling in polarization diversity systems," *IEEE Transactions on Antennas and Propagation*, vol. 55, no. 6, pp. 1709–1715, 2007.

[4] G. R. Maccartney, T. S. Rappaport, S. Sun, and S. Deng, "Indoor office wideband millimeter-wave propagation measurements and channel models at 28 and 73 GHz for ultra-dense 5G wireless networks," *IEEE Access*, vol. 3, pp. 2388–2424, 2015.

[5] Y. Yamaguchi, T. Abe, and T. Sekiguchi, "Experimental study of radio propagation characteristics in an underground street and corridors," *IEEE Transactions on Electromagnetic Compatibility*, vol. 28, no. 3, pp. 148–155, 1986.

[6] B. Y. Toh, R. Cahill, and V. F. Fusco, "Understanding and measuring circular polarization," *IEEE Transactions on Education*, vol. 46, no. 3, pp. 313–318, 2003.

[7] T. Fukusako, "Broadband characterization of circularly polarized waveguide antennas using L-shaped probe," *Journal of Electromagnetic Engineering and Science*, vol. 17, no. 1, pp. 1–8, 2017.

[8] Y. Sung, "Investigation into the polarization of asymmetrical-feed triangular microstrip antennas and its application to reconfigurable antennas," *IEEE Transactions on Antennas and Propagation*, vol. 58, no. 4, pp. 1039–1046, 2010.

[9] Q. Zhu, S. Yang, and Z. Chen, "Modified corner-fed dual-polarised stacked patch antenna for micro-base station applications," *Electronics Letters*, vol. 51, no. 8, pp. 604–606, 2015.

[10] R. Zaker and A. Abdipour, "Dual-wideband circularly-polarised slot antenna using folded L-shaped stub," *Electronics Letters*, vol. 47, no. 6, pp. 361–363, 2011.

[11] C.-Y.-D. Sim, Y.-J. Liao, and H.-L. Lin, "Polarization reconfigurable eccentric annular ring slot antenna design," *IEEE Transactions on Antennas and Propagation*, vol. 63, no. 9, pp. 4152–4155, 2015.

[12] J. M. Kovitz and Y. Rahmat-Samii, "Using thick substrates and capacitive probe compensation to enhance the bandwidth of traditional CP patch antennas," *IEEE Transactions on Antennas and Propagation*, vol. 62, no. 10, pp. 4970–4979, 2014.

[13] Y. Li, S. Sun, and F. Yang, "A miniaturized Yagi-Uda-oriented double-ring antenna with circular polarization and directional pattern," *IEEE Antennas and Wireless Propagation Letters*, vol. 12, pp. 945–948, 2013.

[14] J. S. Row, "Design of square-ring microstrip antenna for circular polarisation," *Electronics Letters*, vol. 40, no. 2, pp. 93–95, 2004.

[15] X. L. Bao and M. J. Ammann, "Compact annular-ring embedded circular patch antenna with cross-slot ground plane for circular polarisation," *Electronics Letters*, vol. 42, no. 4, pp. 192-193, 2006.

[16] Nasimuddin, Z. N. Chen, and X. Qing, "Asymmetric-circular shaped slotted microstrip antennas for circular polarization and RFID applications," *IEEE Transactions on Antennas and Propagation*, vol. 58, no. 12, pp. 3821–3828, 2010.

[17] A. K. Gautam, A. Kunwar, and B. K. Kanaujia, "Circularly polarized arrowhead-shape slotted microstrip antenna," *IEEE Antennas and Wireless Propagation Letters*, vol. 13, pp. 471–474, 2014.

[18] S. B. Vignesh, N. Nasimuddin, and A. Alphones, "Stubs-integrated-microstrip antenna design for wide coverage of circularly polarised radiation," *IET Microwaves, Antennas & Propagation*, vol. 11, no. 4, pp. 444–449, 2017.

[19] A. Narbudowicz, M. J. Ammann, and D. Heberling, "Reconfigurable axial ratio in compact GNSS antennas," *IEEE Transactions on Antennas and Propagation*, vol. 64, no. 10, pp. 4530–4533, 2016.

[20] A. Khidre, K.-F. Lee, F. Yang, and A. Z. Elsherbeni, "Circular polarization reconfigurable wideband E-shaped patch antenna for wireless applications," *IEEE Transactions on Antennas and Propagation*, vol. 61, no. 2, pp. 960–964, 2013.